Co(II) complexes of tetraazamacrocycles appended with amide or hydroxypropyl groups as paraCEST agents

Jaclyn J. Raymond,[a] Samira M. Abozeid,[a‡] Gregory E. Sokolow,[a] Christopher J. Bond,[a] Constance E. Yap,[a] Alexander Y. Nazarenko,[b] Janet R. Morrow[a*]

[a] Department of Chemistry, Natural Sciences Complex, University at Buffalo, the State University of New York, Amherst, NY 14260

[b] Chemistry Department, SUNY College at Buffalo, 1300 Elmwood Ave, Buffalo, NY 14222

‡ Current address: Department of Chemistry, Faculty of Science, Mansoura University, El-Gomhoria Street, 35516 Mansoura, Egypt

ABSTRACT Co(II) complexes of 1,4,7,10-tetraazacyclododecane (CYCLEN) or 1,4,8,11-tetraazacyclotetradecane (CYCLAM) with 2-hydroxypropyl or carbamoylmethyl (amide) pendants are studied with the goal of developing paramagnetic chemical exchange saturation transfer (paraCEST) agents. Single-crystal X-ray diffraction studies show that two of the coordination cations with hexadentate ligands, $[Co(DHP)]^{2+}$ and $[Co(BABC)]^{2+}$, form six-coordinate complexes; whereas two CYCLEN-based complexes with potentially octadentate ligands, $[Co(THP)]^{2+}$ and $[Co(HPAC)]^{2+}$, are seven coordinate with only three of the four pendant groups bound to the metal center. ^{1}H NMR spectra of these complexes suggest that the six-coordinate complexes are present as a single isomer in aqueous solution. For the complexes which are seven-coordinate in the solid state, one is highly fluxional in aqueous solution on the NMR time scale ($[Co(HPAC)]^{2+}$), whereas the NMR spectrum of $[Co(THP)]^{2+}$ is consistent with an eight-coordinate complex with all pendants bound. Co(II) complexes of CYCLEN derivatives show CEST effects of low intensity that are assigned to NH or OH groups of the pendants. One complex, $[Co(DHP)]^{2+}$, shows a highly-shifted CEST peak at 113 ppm versus bulk water, attributed to OH protons. However, the CEST effect is largest for two Co(II) CYCLAM-based complexes with coordinated amide groups that undergo NH proton exchange. All five complexes are inert towards dissociation in buffered solutions containing carbonate and phosphate and towards trans-metalation by excess Zn(II). These data give insight into the production of an intense CEST effect for tetraazamacrocyclic complexes with pendant groups containing NH or OH exchangeable protons. The intense and highly shifted CEST peak(s) of the CYCLAM-based complexes suggest that they are promising for further development as paraCEST agents.

INTRODUCTION

Chemical exchange saturation transfer (CEST) agents have been extensively studied as MRI probes.[1, 2] CEST agents have exchangeable protons, typically from NH or OH groups, that undergo chemical exchange with bulk water under physiologically relevant conditions. An important restriction involves the difference in frequency between the exchangeable proton and bulk water ($\Delta\omega$) which must be greater than the exchange rate constant (k_{ex}).[3] Irradiation with a presaturation pulse at the frequency of the exchangeable proton leads to a decrease in the intensity of the bulk water proton resonance upon exchange of the magnetically saturated proton. CEST agents have the advantage that the signal can be turned on or off by application of the presaturation pulse. Diamagnetic agents with exchangeable protons, typically OH or NH protons of alcohol, amine, or amide functionalities, have been studied as endogenous substances or may be administered as exogenous contrast agents.[1, 4]

CEST agents that contain a paramagnetic metal ion are referred to as paraCEST agents.[1, 5, 6] Paramagnetic metal ion complexes have the advantage of shifting the exchangeable proton far from that of bulk water or tissue to minimize background signal from the magnetization transfer effect. Paramagnetic metal ion complexes are typically divided into two classes based on their exchangeable groups. The most extensively studied class of paraCEST agents has an exchangeable water ligand in nine-coordinate lanthanide (Ln(III)) complexes, with the bound water as a capping ligand in a capped twisted square pyramidal complex.[6] The rate constant for the exchanging water of these Ln(III) based paraCEST agents has been tuned by the incorporation of different pendant groups, mostly to slow down water exchange.[7, 8] The focus on slowing the water exchange rate constant is important towards *in vivo* studies, where the irradiation power is limited by animal safety concerns. The relationship between k_{ex} and the irradiation power (B_1) suggests a k_{ex} of 2700 s^{-1} is optimal for a 10 μT pulse power in preclinical animal studies.[9, 10] A second class of paraCEST agent contains exchangeable protons on ligands, such as OH of hydroxypropyl pendants, NH of amides or amines, or heterocyclic NH groups.[4, 6, 11] These OH and NH protons often exchange more slowly than the bound water of the Ln(III) complexes.[10] ParaCEST agents that contain amides with exchangeable NH groups[6, 12] or OH of hydroxyalkyl pendants[13, 14] are among the most promising choices.

Paramagnetic complexes of Ln(III) and first-row transition metal ions have been studied as paraCEST agents.[4, 11, 15] These coordination complexes have macrocyclic or rigid linear ligands that serve to form kinetically inert complexes in aqueous solutions and under physiologically relevant conditions. However, whereas Ln(III) paraCEST agents are generally limited to the trivalent oxidation state, there are multiple spin and oxidation states that are accessible for first-row transition metal complexes.[11, 15] The accessibility of different states is useful in the formation of responsive agents,[16, 17] but also highlights the need to control spin and oxidation state through coordination chemistry of the transition metal ions. The transition metal complexes that have been most frequently

studied as paraCEST agents include those of high-spin Fe(II), low-spin Fe(III), high-spin Co(II), and Ni(II).[11, 16]

Of the transition metal complexes studied as paraCEST agents, high-spin Co(II) complexes are among the most successful, due to the excellent properties of Co(II) as a shift agent.[18, 19] Macrocyclic ligands that have been studied with Co(II) paraCEST agents include triaza- or tetraza-, mixed oxa-azamacrocycles, or pyridine containing macrocycles[20] that have pendant groups to encapsulate the metal ion in six, seven, or eight-coordinate complexes.[11] The macrocyclic ligands should stabilize the divalent high-spin state of cobalt and confer a large degree of kinetic inertness to dissociation, as well as good water solubility. Moreover, it is important to have a symmetrical complex to produce as many equivalent exchangeable protons as possible. In most cases, a single isomer is preferable to the existence of multiple isomers that produce multiple CEST peaks of smaller intensity. Minimizing dynamic processes that can broaden proton resonances on the NMR timescale is also critical to obtain intense CEST peaks.[21]

Studies in our laboratory have focused on Co(II) paraCEST agents that contain amides appended to 1,4,7-triazacyclononane (TACN),[22-24] CYCLEN,[22, 25, 26] or CYCLAM[22, 25, 27] macrocycles. For TACN and CYCLEN with amide pendants, the complexes are fluxional and these dynamic processes broaden the proton resonances and decrease the CEST effect. CYCLAM complexes with amide pendants are typically not fluxional on the NMR timescale, but often form multiple isomers.[27] Moreover, the symmetry of the CYCLAM complexes of Co(II) may be low and this leads to multiple amide NH resonances. In contrast, Co(II) macrocyclic complexes with homochiral hydroxypropyl pendants are rigid and produce relatively sharp ligand proton resonances.[23, 24, 28] In these complexes, the methyl group of the hydroxypropyl pendant serves to reduce pendant group dynamic processes. However, the CEST peaks attributed to the OH protons of hydroxypropyl are generally not very intense compared to those of amide NH protons. This is attributed to an optimal CEST effect at acidic pH for OH protons of Co(II) complexes and exchange broadening due to rapid exchange at neutral pH.[23] Interestingly, Co(II) complexes of TACN that combine hydroxypropyl and amide groups have sharp CEST signals from amide NH and hydroxypropyl OH protons.[24] The mixed pendant approach is applied here to tetraazamacrocyclic ligands, such as CYCLEN and CYCLAM complexes, in order to capitalize on the additional sites for pendant group attachment to potentially produce a greater number of equivalent protons for CEST experiments. Here we present Co(II) complexes of CYCLEN and CYCLAM derivatives and study the effect of mixed amide and hydroxypropyl pendants on the geometry and structure of the complexes, as well as dynamic solution processes, formation of isomers, and obtaining a strong CEST effect.

Scheme 1. Macrocyclic ligands for Co(II)

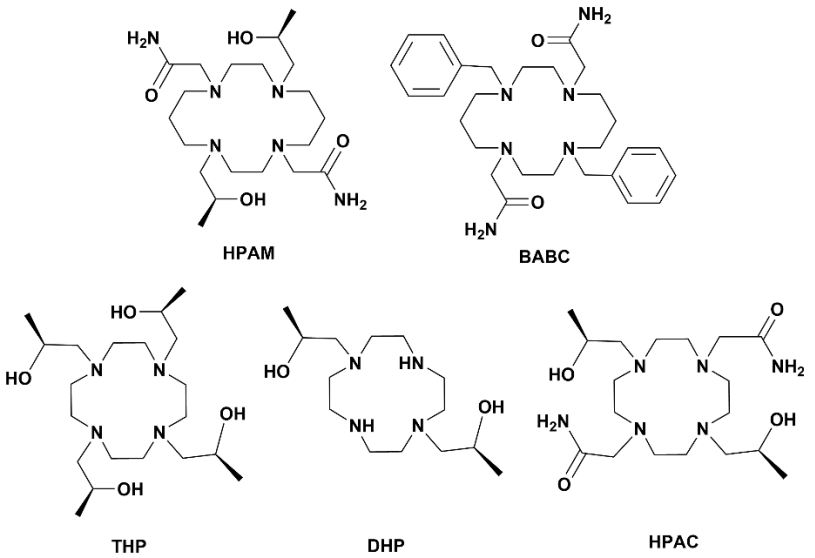

RESULTS and DISCUSSION

Synthesis and Structural Data.

Five tetraazamacrocyclic ligands and their Co(II) complexes were prepared. The 2-hydroxypropyl or carbamoylmethyl (amide) pendants were added to either CYCLAM or CYCLEN. The CYCLEN-based ligands including THP, DHP, and HPAC contain four or two hydroxypropyl pendants, or alternatively a mixture of amide and hydroxypropyl pendants, respectively. The CYCLAM-based ligands HPAM and BABC contain amide-based pendants with either hydroxypropyl pendants or benzyl groups, respectively.

The THP ligand was synthesized by direct alkylation of CYCLEN with *S*-(-)-propylene oxide, following a previously reported procedure.[29] The ligands DHP and HPAC first require the synthesis of a protected precursor, 1,7-bis(benzyl) CYCLEN, which was prepared using a previously established procedure.[30] Upon addition of the 2-hydroxypropyl pendants to 1,7-bis(benzyl) CYCLEN by using *S*-(-)-propylene oxide, catalytic hydrogenation was then performed to remove the benzyl groups to yield the DHP ligand (Scheme S1). The HPAC ligand was prepared by the addition of 2-bromoacetamide to DHP (Scheme S2). The CYCLAM-based ligands HPAM and BABC were synthesized using 1,8-bis(benzyl)-CYCLAM, which was prepared using a previously established procedure.[31] Alkylation of 1,8-bis(benzyl) CYCLAM with 2-bromoacetamide yielded BABC (Scheme S3). The benzyl groups of BABC were removed by using catalytic hydrogenation to prepare 4,11-bis(amide)-CYCLAM (BAC) and the HPAM ligand was

then formed by the addition of the 2-hydroxypropyl pendants to BAC by using *S*-(-)-propylene oxide (Scheme S4).

The Co(II) complexes of the neutral ligands were formed by adding cobalt nitrate hexahydrate ($Co(NO_3)_2 \cdot 6H_2O$) or cobalt chloride hexahydrate ($Co(Cl)_2 \cdot 6H_2O$) in an ethanolic solution to a solution of the respective ligand under argon (Scheme S5). Detailed synthetic procedures can be found in the Supplementary Information. The complexes prepared with $CoCl_2$ were used to grow crystals for X-ray diffraction studies, whereas the complexes prepared with $Co(NO_3)_2$ were used for all further solution studies and for CEST experiments. The effective magnetic moments (μ_{eff}) of the isolated Co(II) complexes prepared from the nitrate salts are consistent with high-spin Co(II), as determined by the Evans method. The μ_{eff} values for the complexes are within the literature range of 4.2 to 5.2 B.M. for high-spin Co(II) complexes (S = 3/2) of octahedral geometry (see Table 1). The Co(II) complexes were crystallized from slow evaporation of acetonitrile (see Figure 1 below).

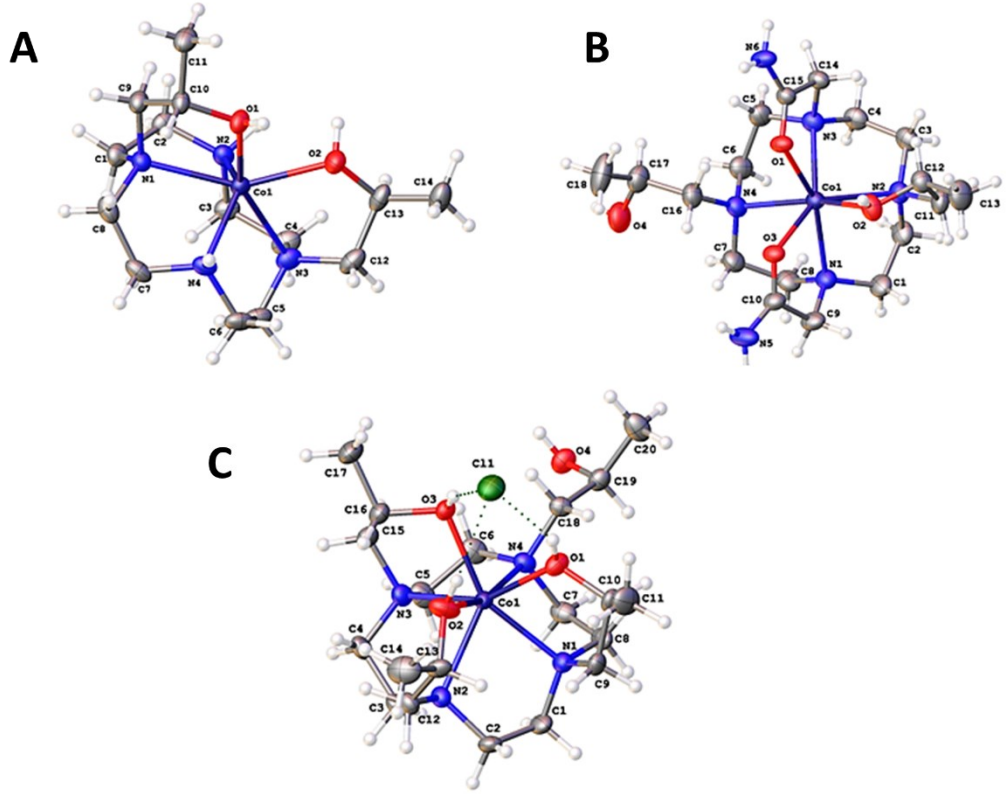

Figure 1. Crystal structures of complex cations for $[Co(DHP)]^{2+}$ (A), $[Co(HPAC)]^{2+}$ (B), and $[Co(THP)]^{2+}$ showing a chloride counter ion (C). Most counter-ions have been omitted for clarity. Thermal ellipsoids drawn at 50% probability.

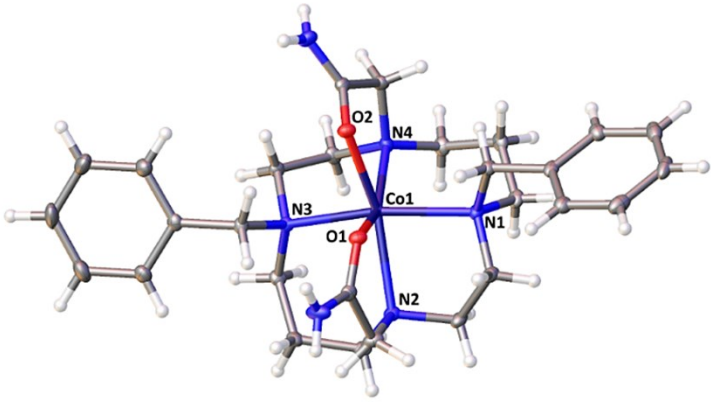

Figure 2. Crystal structure of the complex cation for $[Co(BABC)]^{2+}$ with counter-ions and solvent omitted for clarity. Thermal ellipsoids are drawn at 50% probability.

CYCLEN-based complexes of Co(II) with four pendants commonly form 7-coordinate complexes.[26] The crystal structures of the tetra-substituted CYCLEN-based complexes $[Co(HPAC)]^{2+}$ (Figure 1B) and $[Co(THP)]^{2+}$ (Figure 1C) are both seven-coordinate, with three of the four pendants and all four N-donors of the macrocycle bound to the metal center. The coordination polyhedra of these seven-coordinate complexes are prismatoids with seven vertices (Figures S24, S25, S28, and S29), with three oxygen atoms of pendant groups located in an upper trigonal face and four nitrogen atoms of the macrocycle forming a rhombic lower face. The Co(II) complex of the hexadentate DHP ligand (Figure 1A) is 6-coordinate with all four N-donors of the macrocycle and the oxygen atoms of both hydroxypropyl pendants bound to the metal center, of which the bound oxygens are positioned in a *cis*- arrangement above the plane of the four nitrogen atoms of the macrocycle. The geometry of this complex is best described as a distorted wedge with six vertices (Figure S26 and S27). The crystallographic data can be found in Table S4, as well as selected bond lengths (Tables S5-S7) and selected bond angles (Tables S9-S11).

The CYCLAM-based complex $[Co(BABC)]^{2+}$ is six-coordinate with four coordinated nitrogen donors of the macrocyclic backbone and two oxygen donors from the pendant amide groups (Figure 2). This complex has the rare *cis*-geometry for the amide pendant groups. In this geometry, the Co(II) ion is substantially above the centroid of the plane formed by the four nitrogen atoms and the complex cation has the folded *cis*-I configuration with all nitrogen pendant groups oriented up. An analogous Co(II) complex of CYCLAM appended with four amide groups shows 1,4-*trans* or 1,8-*trans* geometry.[27] However, the Co(II) complex of 1,8-bis(benzyl)-4,11-bis-(2-hydroxypropyl)-CYCLAM has the 1,8-pendents in *cis*-geometry, analogous to $[Co(BABC)]^{2+}$.[28] Comparison of these examples suggests that the bulky benzyl groups promote the formation of the folded *cis*-I configuration. Selected bond lengths and bond angles can be found in Tables S8 and S11, respectively.

Spectroscopic Characterization.

Electronic absorbance spectra of the complexes were collected in aqueous solutions of the respective complex at 37 °C. Typically, high-spin hexacoordinate Co(II) (d^7) complexes of octahedral geometry display three d-d electronic transitions.[32] Each of the complexes exhibits three major electronic absorption peaks between 400 to 600 ppm, shown in Figure S20, which are assigned to spin-allowed, Laporte-forbidden d-d transitions. The calculated molar absorptivity (ε) values for the respective absorption bands of the Co(II) complexes (Tables S2 and S3) are consistent with those of bands corresponding to d-d transitions for complexes of pseudo-octahedral geometry, for which typically ε is less than 100 $M^{-1}\,cm^{-1}$.[23] Notably, $[Co(BABC)]^{2+}$ and $[Co(HPAM)]^{2+}$ display very similar d-d electronic absorbances, consistent with NMR spectra that suggests similar solution structures as described below.

CYCLAM-based complexes of Co(II) have several different common isomeric forms, which can be identified through comparison of their ^1H NMR spectra.[25, 27] Tetra-alkylated CYCLAM-based complexes with first-row transition metals can adopt various conformations, including isomers with two pendants arranged either in a *cis*- or *trans*-configuration.[22, 33] The coordinating pendants may be either 1,4- or 1,8- derivatives.[27] The ^1H NMR spectrum of $[Co(BABC)]^{2+}$ shows fourteen paramagnetically shifted proton resonances, in addition to the barely shifted phenyl ring resonances, consistent with apparent C_2 symmetry (see Figure 3 below). The ^1H NMR spectrum of $[Co(BABC)]^{2+}$ resembles that of the analogous Co(II) complex of 1,8-bis(benzyl)-4,11-bis(2-hydroxypropyl)-CYCLAM that contains hydroxypropyl groups instead of amide donor groups in the same *cis*-pendant configuration.[28] The $[Co(HPAM)]^{2+}$ complex shows paramagnetically shifted resonances in the same general region of the spectrum as those of $[Co(BABC)]^{2+}$, consistent with a similar geometry (Figure 3). However, there are approximately 26 proton resonances, which vary in intensity, thus indicating the presence of two isomers in inequal concentrations. Since the additional set of proton resonances is not shifted greatly from that of the main isomer which has resonances similar to $[Co(BABC)]^{2+}$, we propose that the additional isomer results from distinct hydroxypropyl group configurations within the coordination sphere.

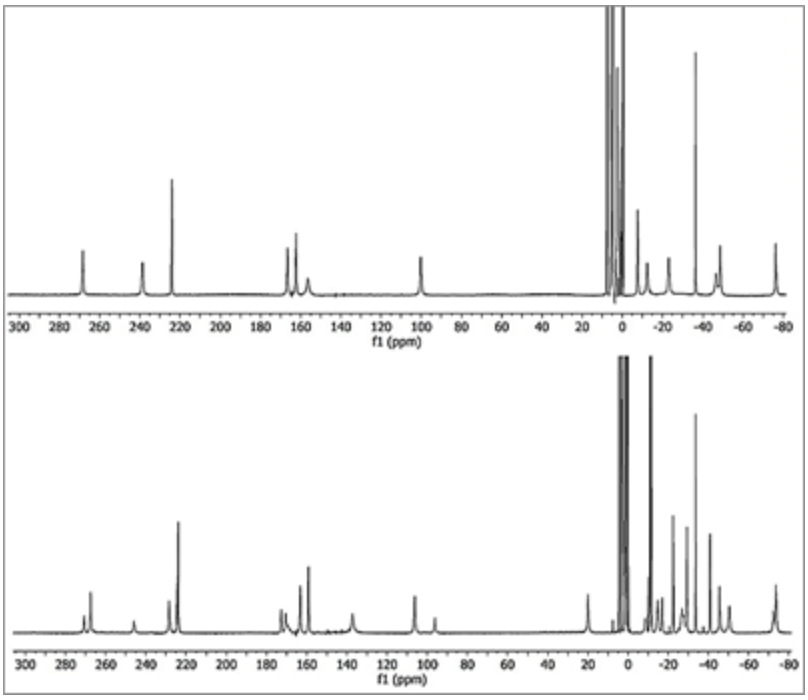

Figure 3. ^{1}H NMR spectra for the CYCLAM-based complexes $[Co(BABC)]^{2+}$ (top) and $[Co(HPAM)]^{2+}$ (bottom). The samples contained 20 mM complex in D_2O at 25 °C.

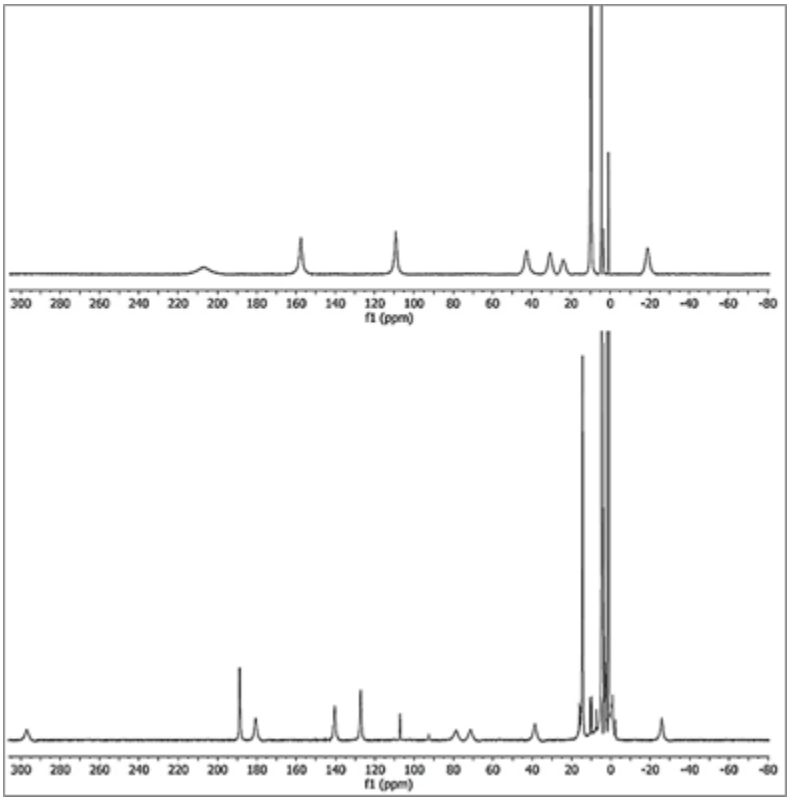

Figure 4. ^{1}H NMR spectra for the CYCLEN-based complexes $[Co(THP)]^{2+}$ (top) and $[Co(DHP)]^{2+}$ (bottom). The samples contained 20 mM complex in D_2O at 25 °C.

The ^{1}H NMR spectra of the CYCLEN-based complexes $[Co(THP)]^{2+}$ and $[Co(DHP)]^{2+}$ are consistent with the presence of a single diastereomer in solution, based on the number of paramagnetically shifted proton resonances (see Figure 4 above). $[Co(THP)]^{2+}$ produces eight paramagnetically-shifted, nonexchangeable proton resonances from -20 to +210 ppm. Four of the resonances for $[Co(THP)]^{2+}$ correspond to the methylene protons of the macrocyclic backbone and four additional resonances are due to the non-exchangeable protons of the hydroxypropyl pendants. The number of proton resonances is consistent with four-fold symmetry of the complex, with the four hydroxypropyl pendants being equivalent and bound to the metal center to give an 8-coordinate complex in solution. This differs from the solid-state structure, which is seven-coordinate. However, solution studies of the analogous Fe(II) complex, $[Fe(THP)]^{2+}$, are consistent with an eight-coordinate complex in solution[34] and a related Fe(II) complex with four appended amide groups is eight-coordinate, as shown by X-ray crystallography.[25] For $[Co(DHP)]^{2+}$, twelve resonances are observed in the range of -25 to +300 ppm. Four proton resonances are attributed to the two sets of four inequivalent, nonexchangeable protons of the hydroxypropyl pendants, while the additional eight resonances are assigned to protons of the macrocycle. In contrast, the mixed amide hydroxypropyl pendant containing complex, $[Co(HPAC)]^{2+}$, exhibits highly broadened resonances that shift and merge with temperature (Figure S1). Such highly broadened resonances are typical for Co(II) complexes of CYCLEN containing amide pendants,[22] due to dynamic processes. Most likely the dynamic process interconverts between two diastereomers involving the CYCLEN backbone configuration (ΔΔΔΔ or ΛΛΛΛ).[25, 35] In any case, the solution structure of $[Co(HPAC)]^{2+}$ is more fluid than that of $[Co(THP)]^{2+}$, which contains only hydroxypropyl pendants.

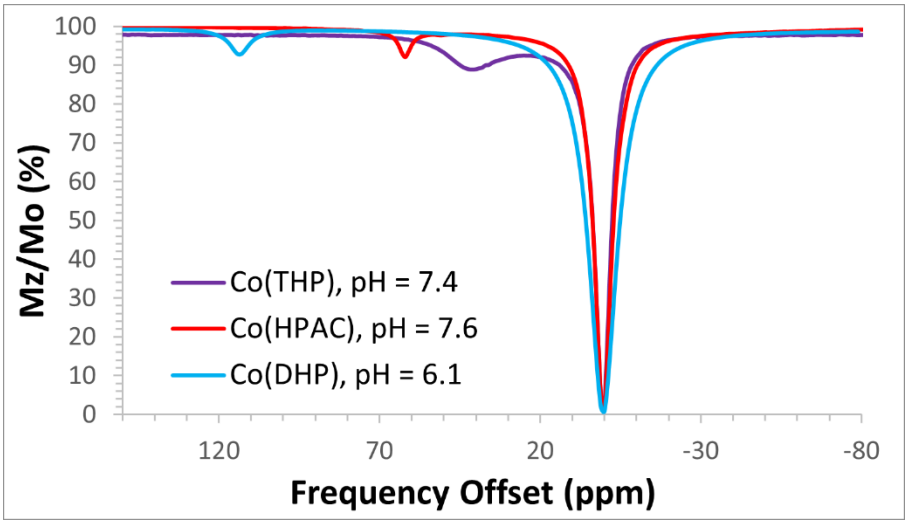

Figure 5. CEST spectra overlay for the CYCLEN-based complexes $[Co(THP)]^{2+}$ (pH = 7.4), $[Co(HPAC)]^{2+}$ (pH = 7.6), and $[Co(DHP)]^{2+}$ (pH = 6.1) at T = 37 °C. Samples contained 10 mM complex, 100 mM NaCl, and 20 mM HEPES buffer. B_1 = 24 μT applied for 2 s.

Z-Spectra and CEST Effect.

The CEST spectra (or Z-spectra) were acquired for each of the complexes and are plotted as the percent decrease in bulk water resonance intensity (M_Z/M_o %) as a function of the presaturation frequency (ppm).[5] $[Co(THP)]^{2+}$ exhibits one CEST peak at 42 ppm, corresponding to a single, equivalent set of OH protons (Figure 5 above) from the four hydroxypropyl pendants. $[Co(DHP)]^{2+}$ gives a more highly shifted, but weak CEST peak at 113 ppm (Figure 5), which could be attributed to either the OH protons of the two hydroxypropyl pendants or the NH protons of the macrocycle. The mixed pendant containing complex $[Co(HPAC)]^{2+}$ possesses two sets of exchangeable protons, OH or NH, but only exhibits one CEST peak at 62 ppm (Figure 5). To gain further information about CEST peak assignments (OH or NH protons), the pH dependence of the CEST experiments was varied from 6 to 8 (Figure S9).

For transition metal complexes, the CEST effect for amide protons typically is base-catalyzed and optimized at higher pH values,[26, 27] whereas the OH protons of the hydroxypropyl pendants are optimized at lower pH values.[23] The CEST peak intensity is expected to increase over this pH range of 6 to 7.5 for amide pendants, but not for hydroxypropyl OH protons. The CEST peak for $[Co(HPAC)]^{2+}$ was optimized at pH = 7.8, which is consistent with NH exchange of the amide pendant. Similarly, CEST experiments at various pH values were also carried out for $[Co(THP)]^{2+}$ and $[Co(DHP)]^{2+}$ between pH values of 5.3 to 7.3 and 5.0 to 7.3, respectively (Figures S7 and S8). The CEST peaks for these complexes were optimized at relatively lower pH values of 6.8 and 6.4 for $[Co(THP)]^{2+}$ and $[Co(DHP)]^{2+}$, respectively, which is typical for OH protons of hydroxypropyl pendants. Thus, the CEST peak exhibited by the hexacoordinate complex $[Co(DHP)]^{2+}$ likely corresponds to the OH protons of the pendants rather than the NH protons of the macrocyclic backbone. Based on the optimized intensity values from the pH-dependence studies, a summary of the CEST peak shifts ($\Delta\omega$) (ppm), intensity (% CEST), and the respective sample pH can be found in Table 1 below.

Table 1. Summary of data for the complexes: effective magnetic moment (μ_{eff}) (B.M.), CEST peak shift ($\Delta\omega$) (ppm), intensity of the CEST peak (%), and the pH of the respective sample. All solutions contained 10 mM complex.

Complex	μ_{eff} (B.M.)	$\Delta\omega$ (ppm)	CEST (%)	pH
$[Co(THP)]^{2+}$	4.44 ± 0.06	42	12	6.8
$[Co(DHP)]^{2+}$	4.57 ± 0.05	113	5	6.4
$[Co(HPAC)]^{2+}$	4.86 ± 0.05	62	7	7.5
$[Co(HPAM)]^{2+}$	4.56 ± 0.04	99, 102	19	7.6
$[Co(BABC)]^{2+}$	4.36 ± 0.09	102	31	7.6

CEST spectra for the CYCLAM-based complexes $[Co(BABC)]^{2+}$ and $[Co(HPAM)]^{2+}$ were obtained. One CEST peak is observed for $[Co(BABC)]^{2+}$ at 102 ppm over a pH range of 6.0-8.1 (Figures 6 and S4), whereas two peaks are observed for $[Co(HPAM)]^{2+}$ at 99 and 102 ppm over a pH range of 6.6 to 7.6 (Figures 7 and S5). The single CEST peak observed for $[Co(BABC)]^{2+}$ is attributed to the amide pendant NH protons. This is confirmed by the ^{1}H NMR spectrum in DMSO-d_6 that show proton resonances at 114 and 10 ppm versus tetramethylsilane (TMS), which disappear upon addition of D_2O for $[Co(BABC)]^{2+}$ (Figure S2). Presumably, the proton resonance close to bulk water will be obscured by the bulk water peak in the Z-spectrum. On the other hand, $[Co(HPAM)]^{2+}$ contains two sets of exchangeable protons, NH or OH, from the amide pendants or hydroxypropyl pendants. The two observed CEST peaks for this complex are likely from the amide pendant NH protons. This is assigned based on their similarity in position and intensity to those of $[Co(BABC)]^{2+}$, as well as because they are optimized at pH 7.6, which is typical for NH protons as described above. The ^{1}H NMR spectrum of $[Co(HPAM)]^{2+}$ in DMSO-d_6 is also consistent with two exchangeable protons of slightly different intensities at approximately 110 and 114 ppm versus TMS (Figure S3). In addition, there are three exchangeable protons close to the bulk water resonance that disappear upon addition of D_2O. The two CEST peaks of $[Co(HPAM)]^{2+}$ correspond to the two peaks at about 110 and 114 ppm and are assigned as the two amide NH protons of the two isomers. At pH 7.0, the CEST peak at approximately -7 ppm begins to resolve from the bulk water peak. As the pH increases to 7.4 and 7.6, this peak becomes more resolved. However, it is not observed at pH 8.1, likely because the exchange rate becomes too fast. For the sample at pH = 7.4, CEST spectra were also recorded at various saturation power values (B_1 = 12, 19, and 22 μT), for which the peak at -7 ppm becomes more visible as the saturation power decreases (Figure 8). At 12 μT, a peak at ~3 ppm is visible close to the bulk water peak. The CEST peaks at -7 and 3 ppm are most likely additional amide protons given the pH dependence, although we cannot rule out CEST from the unbound hydroxypropyl OH groups. These additional slightly shifted CEST peaks are consistent with related complexes of Co(II) or Fe(II) with bound carbamoylmethyl pendants that show CEST peaks for the two protons on a single amide that are 80 ppm different.[36] For the Fe(II) complexes, this large chemical shift change has been attributed to differences in spin density transfer at the two distinct NH protons of the pendant.[37]

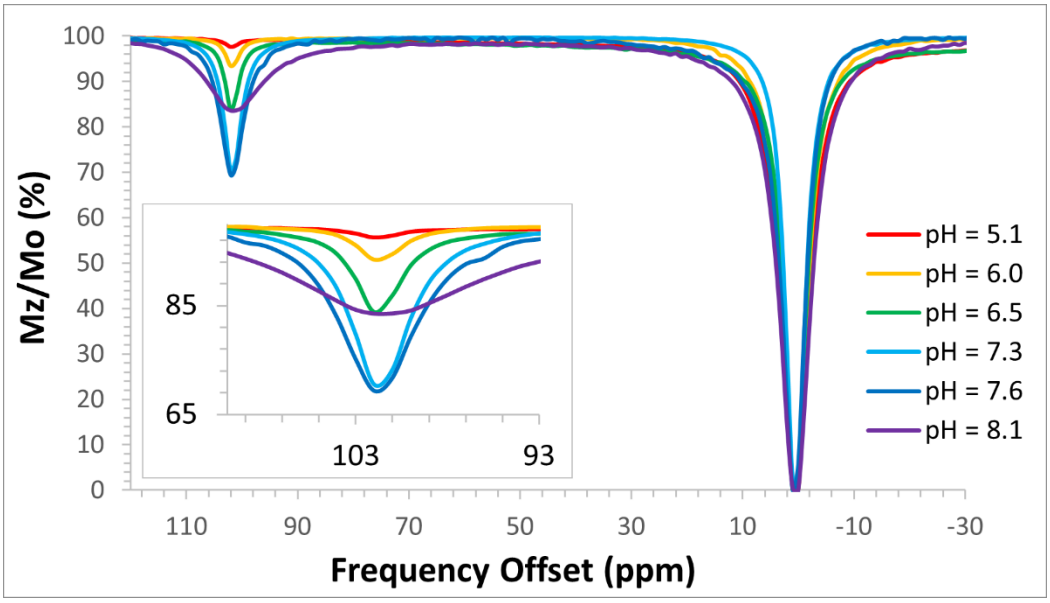

Figure 6. CEST spectra overlay showing pH-dependence of $[Co(BABC)]^{2+}$ at 37 °C. Samples contained 10 mM complex, 20 mM HEPES buffer, and 100 mM NaCl. B_1 = 22 µT, applied for 2.4 seconds.

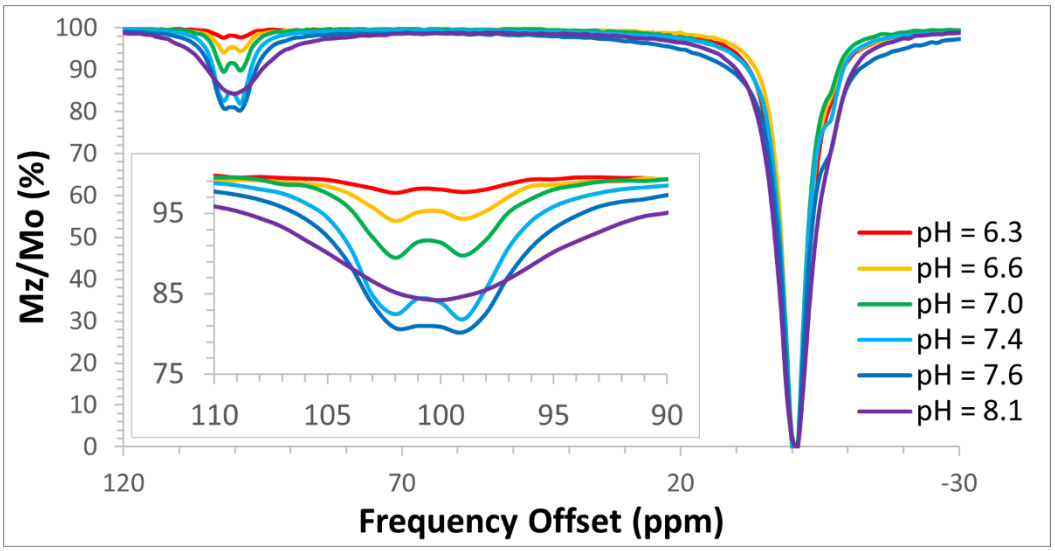

Figure 7. CEST spectra overlay showing pH-dependence of $[Co(HPAM)]^{2+}$ at 37 °C. Samples contained 10 mM complex, 20 mM HEPES buffer, and 100 mM NaCl. B_1 = 22 µT, applied for 2.4 seconds.

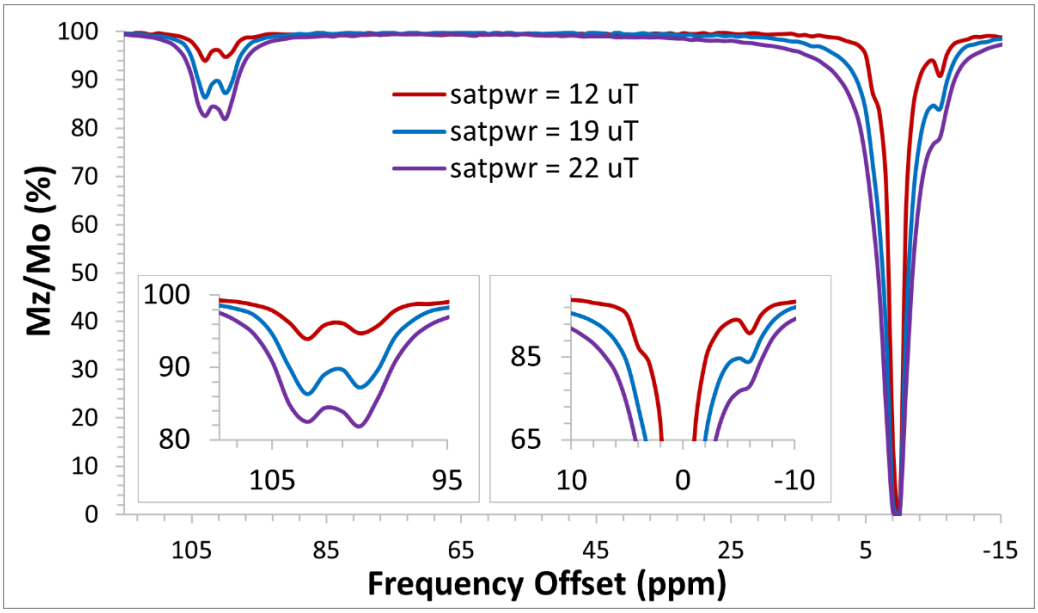

Figure 8. CEST spectra overlay at various saturation power values (12, 19, and 22 μT) for $[Co(HPAM)]^{2+}$ at T = 37 °C and pH = 7.4. Samples contained 10 mM complex, 20 mM HEPES buffer, and 100 mM NaCl. The radiofrequency pulse was applied for 2.4 seconds.

These studies show that Co(II) complexes of CYCLAM derivatives with amide pendants are the more promising of the complexes studied here, as they show highly shifted CEST peaks of strong intensity.[22, 27] We previously reported on Co(II) complexes of tetrasubstituted CYCLAM with amide pendants that have 1,4-*trans*-amide coordination and upon heating, 1,8-*trans*-coordinated amide pendants.[27] The CEST peak intensity of the 1,8-*trans*-derivative is less than that of $[Co(BABC)]^{2+}$ when taken at the same presaturation power, most likely due to lower symmetry of the complex that gives rise to four CEST peaks. The fact that there is apparently a single CEST peak for $[Co(BABC)]^{2+}$ is consistent with the two pendant amide groups being equivalent in solution. Two symmetrically coordinated amide pendants are predicted to give two sets of CEST peaks, given that the two protons on each amide pendant are inequivalent and do not interconvert due to restricted rotation about the C-N bond. Thus, we observe one CEST peak shifted far from the bulk water resonance, while one set of amide resonances gives rise to a CEST peak which is obscured by the bulk water peak. The assignment of exchangeable NH protons by NMR spectroscopy suggests that the two sets of amide protons are at approximately 100 ppm different. The $[Co(HPAM)]^{2+}$ complex shows additional CEST peaks that are close to the bulk water signal, which are attributed to either the amide NH protons or an unbound hydroxypropyl group.

To further characterize the paraCEST agents, the exchange rate constants for OH groups in $[Co(THP)]^{2+}$ or NH groups in $[Co(BABC)]^{2+}$ were determined. These two complexes were chosen based on their intense CEST peaks that can be readily studied

as a function of pulse power for determination of k_{ex} in an Omega Plot.[8, 10] For $[Co(THP)]^{2+}$, the k_{ex} was 12,600 s^{-1} at pH 6.8, but exchange was too rapid to measure at the physiological pH of 7.4 (Figures S13, S14, and S19; Table S1). For $[Co(BABC)]^{2+}$, k_{ex} increased with pH to give rate constants of 1070, 1670, and 4740 at pH 6.8, 7.2, and 7.4, respectively (Figures S10-S12 and S16-S18; Table S1). Thus, k_{ex} for $[Co(THP)]^{2+}$ hydroxyl protons is too fast under physiological conditions even at high pulse powers, whereas the rate constants for $[Co(BABC)]^{2+}$ are in an optimal range for irradiation by medium to low radiofrequency pulse powers. Based on discussions of pulse power restrictions for *in vivo* studies, a k_{ex} of 2,700 s^{-1} is an optimal value for a 10 uT pulse which is tolerated in animals.[9, 10] In fact, $[Co(BABC)]^{2+}$ shows a CEST effect of about 8% at the 10 μT power (Figure S10).

Kinetic Inertness to Dissociation.

Kinetic studies for monitoring complex dissociation were performed by using UV-vis spectroscopy to monitor the change in absorbance for the corresponding absorption bands of the complex in the presence of competing cations including excess Zn^{2+} (Figure S21), biologically-relevant anions (13 mM CO_3^{2-}, 0.2 mM PO_4^{3-}, and 50 mM Cl^-) (Figure S22), and under acidic conditions (Figure S23) for at least 22 hours at 37 ºC. Studies showed that $[Co(THP)]^{2+}$ was inert to dissociation in the presence of excess Zn^{2+} (1:3 complex to Zn^{2+}) (Figure S21A), in the buffered solutions containing anions (Figure S22A), and even in 2 M acid (Figure S23A). In contrast, $[Co(BABC)]^{2+}$ produced spectra consistent with dissociation in acidic solutions (0.1 M) over several hours (Figure S23B). Both CYCLAM complexes, $[Co(BABC)]^{2+}$ and $[Co(HPAM)]^{2+}$, were resistant to trans-metalation with Zn(II) over more than an hour (Figures S21D and S21E). However, over a period of 24 hours these complexes showed evidence of trans-metalation to give 50% and 35% remaining Co(II) complex. The fact that there is no further loss of Co(II) complex at 48 or 23 hours, respectively, is most likely due to an equilibrium established between the Zn(II) and Co(II) complexes. At an initial ratio of 1:3 complex to Zn^{2+}, and then an additional 4 equivalents of Zn^{2+} after 30 minutes, $[Co(DHP)]^{2+}$ appears resistant to loss of complex (Figure S21B). $[Co(HPAC)]^{2+}$ also appears inert to trans-metalation in the presence of excess Zn^{2+} over 24 hours (Figure S21C). All complexes are inert to loss of Co(II) in the presence of anions found in the blood at 37 ºC over 24 hours. However, the slight increase and change of peaks maxima in the UV-vis spectrum of $[Co(DHP)]^{2+}$ and $[Co(HPAC)]^{2+}$ suggest that there is a change in solution structure.

CONCLUSIONS

Effective paraCEST agents require highly shifted CEST peaks that are far from that of bulk water (> 80 ppm) to bypass magnetization transfer interference from tissue.[4, 38, 39] In the study here, this condition is met by three of the five Co(II) complexes, including one CYCLEN and two CYCLAM complexes. Not surprisingly, all of the complexes with

highly shifted CEST peaks are six-coordinate, as these complexes are expected to have larger paramagnetic contributions to the proton shifts. Six-coordinate complexes have shorter bond lengths that may lead to greater dipolar (through space) contributions to paramagnetic induced proton shifts. Moreover, the six-coordinate complexes may have greater contact shift contributions between Co(II) and macrocyclic ligand.[18, 19]

A second requirement to optimize the CEST peak intensity for a greater signal in solution, and ultimately *in vivo*, is not so easily met. CEST agents are generally 10-fold less sensitive than Gd(III) MRI contrast agents.[6] For the CEST agent signal intensity, there are many factors that are important, including the radiofrequency pulse power, the duration of the pulse and the number of repetitions, the exchange rate constant, the number of equivalent exchangeable protons, and the type of exchangeable proton.[3, 4] The best type of ligand donor groups here for effective CEST at neutral pH are the amide NH groups in Co(II) complexes. For example, the k_{ex} for $[Co(BABC)]^{2+}$ amide NH groups at pH 7.2, 37 ^{o}C is 1670 s^{-1}, close to the optimal value for a CEST agent at a pulse power of 10 μT (Figures S11 and S17). Other successful examples of Co(II) paraCEST agents are based on complexes with amide NH groups in macrocycles[20] or linear chelates.[40] Additional ligand groups with exchangeable NH protons that produce CEST for transition metal complexes, but are not as intense, include imidazoles,[41, 42] pyrazoles,[43] or aminopyridine groups.[44] The biggest disadvantage to the heterocyclic pendants is that the exchange rate is too rapid and is optimized at low pH values. Hydroxyl OH groups, while promising on Ln(III) complexes, are less promising on Co(II) complexes from the standpoint of the low intensity peaks that are optimized at acidic pH.[23, 28] For example, the $[Co(THP)]^{2+}$ complex studied here has a k_{ex} for the OH groups of 12,600 s^{-1} at pH 6.8 (Figures S13 and S19). The CEST peak decreases in intensity due to exchange broadening at neutral pH for $[Co(THP)]^{2+}$.

The lack of examples of *in vivo* studies of paraCEST agents has recently been discussed.[6] In large part, this is attributed to low sensitivity of the paraCEST agents. Moreover, the extreme responsiveness of paraCEST agents to environment may make it more difficult to study them *in vivo*. For example, Ln(III) agents[45] with exchangeable water or Co(II), Fe(II), or Ni(II) agents[36] with exchangeable amide NH groups all showed an increase in k_{ex} in the presence of serum albumin. The few *in vivo* studies of paraCEST agents feature Ln(III) complexes with a hydroxypropyl group[13] or Ln(III) complexes with an exchangeable water ligand.[46] In these examples, mice were injected with 10- to 20-fold higher doses than typical of Gd(III) agents. However, these *in vivo* examples feature complexes with a single OH or a single water to produce the CEST peak. Solutions to overcome the low sensitivity of paraCEST agents generally include attachment of multiple metal complexes to nanoparticles such as micelles,[47, 48] silica particles,[49, 50] or dendrimers[51] to give agents that contain multiple paraCEST agents in one entity. For these endeavors, there is a need for water-soluble paraCEST agents that have strong

CEST signals from multiple protons in complexes that are easily functionalized. The Co(II) macrocyclic complexes studied here are promising examples for further functionalization towards *in vivo* studies.

Conflicts of Interest. There are no conflicts of interest to declare.

Author Contributions. JJR: manuscript preparation and editing, synthesis and data collection; SMA and CJB: synthesis and data collection; GES: crystallography; CEY: data collection; AYN: crystallography; JRM: manuscript preparation and editing.

Acknowledgements. JRM thanks the NSF (CHE-2004135) for support of our research on paraCEST MRI probes. The authors would like to thank the Chemistry Instrument Center and Magnetic Resonance Center at the University at Buffalo. This work utilized ICP-MS and FTMS that was purchased with funding from a NSF Major Research Instrumentation Program (NSF CHE-0959565) and National Institutes of Health and the Bruker 500 MHz NMR (NSF CHE-2018160). The authors would like to thank SUNY Fredonia and Dr. Allan J. Cardenas for the use of their X-ray diffractometer.

References.

1. *Chemical Exchange Saturation Transfer Imaging: Advance and Applications*, Pan Standford, singapore, 2017.
2. L. Knutsson, J. D. Xu, A. Ahlgren and P. C. M. van Zijl, *Magn Reson Med*, 2018, **80**, 1320-1340.
3. P. C. M. van Zijl and N. N. Yadav, *Magn Reson Med*, 2011, **65**, 927-948.
4. S. Viswanathan, Z. Kovacs, K. N. Green, S. J. Ratnakar and A. D. Sherry, *Chem Rev*, 2010, **110**, 2960-3018.
5. S. R. Zhang, M. Merritt, D. E. Woessner, R. E. Lenkinski and A. D. Sherry, *Acc Chem Res*, 2003, **36**, 783-790.
6. A. D. Sherry, D. D. Castelli and S. Aime, *NMR Biomed*, 2022, DOI: ARTN e4698 10.1002/nbm.4698.
7. W. S. Fernando, A. F. Martins, P. Y. Zhao, Y. K. Wu, G. E. Kiefer, C. Platas-Iglesias and A. D. Sherry, *Inorg Chem* 2016, **55**, 3007-3014.
8. A. D. Sherry and Y. K. Wu, *Curr Opin Chem Biol*, 2013, **17**, 167-174.
9. T. Gambino, V. Laura, P. Perez-Lourido, D. Esteban-Gomez, M. Zaiss, C. Platas-Iglesias and G. Angelovski, *Inorg Chem Front*, 2020, **7**, 2274-2286.
10. A. Rodriguez-Rodriguez, M. Zaiss, D. Esteban-Gomez, G. Angelovski and C. Platas-Iglesias, *Int Rev Phys Chem*, 2021, **40**, 51-79.
11. J. R. Morrow, M. S. I. Chowdhury, S. M. Abozeid, A. Patel, A.; J. J. Raymond, "Transition metal ParaCEST, LipoCEST and CellCEST agents as MRI probes" chapter in the *Encyclopedia of Inorganic and Bioinorganic Chemistry*; Scott, R. A. and Storr, T.; Ed.; John Wiley & Sons, DOI: 10.1002/9781119951438.eibc2749, 1-19.

12. S. Aime, A. Barge, D. Delli Castelli, F. Fedeli, A. Mortillaro, F. U. Nielsen and E. Terreno, *Magn Reson Med*, 2002, **47**, 639-648.
13. G. Ferrauto, E. Di Gregorio, V. Auboiroux, M. Petit, F. Berger, S. Aime and H. Lahrech, *NMR Biomed*, 2018, **31**.
14. I. M. Carnovale, M. L. Lolli, S. C. Serra, A. F. Mingo, R. Napolitano, V. Boi, N. Guidolin, L. Lattuada, F. Tedoldi, Z. Baranyai and S. Aime, *Chem Commun*, 2018, **54**, 10056-10059.
15. A. Gupta, P. Caravan, W. S. Price, C. Platas-Iglesias and E. M. Gale, *Inorg Chem*, 2020, **59**, 6648-6678.
16. J. R. Morrow, J. J. Raymond, M. S. I. Chowdhury and P. R. Sahoo, *Inorg Chem*, 2022, **61**, 14487-14499.
17. S. M. Pinto, V. Tome, M. J. F. Calvete, M. M. C. A. Castro, E. Toth and C. F. G. C. Geraldes, *Coordin Chem Rev*, 2019, **390**, 1-31.
18. I. Bertini, P. Turano and A. J. Vila, *Chem Rev*, 1993, **93**, 2833-2932.
19. I. Bertini, C. Luchinat, G. Parigi and E. Ravera, *NMR of Paramagnetic Molecules: Applications to Metallobiomolecules and Models, 2nd Edition*, 2017, DOI: 10.1016/B978-0-444-63436-8.00001-6, 1-24.
20. R. N. Pradhan, S. Chakraborty, P. Bharti, J. Kumar, A. Ghosh and A. K. Singh, *Dalton Trans*, 2019, **48**, 8899-8910.
21. S. J. Dorazio, A. O. Olatunde, P. B. Tsitovich and J. R. Morrow, *J Biol Inorg Chem*, 2014, **19**, 191-205.
22. S. J. Dorazio, A. O. Olatunde, J. A. Spernyak and J. R. Morrow, *Chem Commun*, 2013, **49**, 10025-10027.
23. S. M. Abozeid, E. M. Snyder, T. Y. Tittiris, C. M. Steuerwald, A. Y. Nazarenko and J. R. Morrow, *Inorg chem* 2018, **57**, 2085-2095.
24. A. Patel, S. M. Abozeid, P. J. Cullen and J. R. Morrow, *Inorg Chem*, 2020, **59**, 16531-16544.
25. A. O. Olatunde, C. J. Bond, S. J. Dorazio, J. M. Cox, J. B. Benedict, M. D. Daddario, J. A. Spernyak and J. R. Morrow, *Chem-Eur J*, 2015, **21**, 18290-18300.
26. C. J. Bond, G. E. Sokolow, M. R. Crawley, P. J. Burns, J. M. Cox, R. Mayilmurugan and J. R. Morrow, *Inorganic chemistry*, 2019, **58**, 8710-8719.
27. C. J. Bond, R. Cineus, A. Y. Nazarenko, J. A. Spernyak and J. R. Morrow, *Dalton Trans*, 2020, **49**, 279-284.
28. S. M. Abozeid, D. Asik, G. E. Sokolow, J. F. Lovell, A. Y. Nazarenko and J. R. Morrow, *Angew Chem Int Ed*, 2020, **132**, 12191-12195.
29. K. O. A. Chin, J. R. Morrow, C. H. Lake and M. R. Churchill, *Inorg Chem*, 1994, **33**, 656-664.
30. A. Rodríguez-Rodríguez, M. Regueiro-Figueroa, D. Esteban-Gómez, T. Rodríguez-Blas, V. Patinec, R. Tripier, G. Tircsó, F. Carniato, M. Botta and C. Platas-Iglesias, *Chemistry – A European Journal*, 2017, **23**, 1110-1117.
31. G. Royal, V. Dahaoui-Gindrey, S. Dahaoui, A. Tabard, R. Guilard, P. Pullumbi and C. Lecomte, *Eur J Org Chem* , 1998, **1998**, 1971-1975.
32. P. Pietrzyk, M. Srebro, M. Radon, Z. Sojka and A. Michalak, *J Phys Chem A*, 2011, **115**, 2316-2324.

33. G. M. Freeman, E. K. Barefield and D. G. Vanderveer, *Inorg Chem*, 1984, **23**, 3092-3103.
34. S. J. Dorazio and J. R. Morrow, *Inorg Chem*, 2012, **51**, 7448-7450.
35. P. B. Tsitovich and J. R. Morrow, *Inorg Chim Acta*, 2012, **393**, 3-11.
36. A. O. Olatunde, J. M. Cox, M. D. Daddario, J. A. Spernyak, J. B. Benedict and J. R. Morrow, *Inorg Chem*, 2014, **53**, 8311-8321.
37. B. Martin and J. Autschbach, *Phys Chem Chem Phys*, 2016, **18**, 21051-21068.
38. C. K. Jones, A. X. Li, M. Suchy, R. H. E. Hudson, R. S. Menon and R. Bartha, *Magn Reson Med*, 2010, **63**, 1184-1192.
39. N. McVicar, A. X. Li, M. Suchy, R. H. E. Hudson, R. S. Menon and R. Bartha, *Magn Reson Med*, 2013, **70**, 1016-1025.
40. A. E. Thorarinsdottir, S. M. Tatro and T. D. Harris, *Inorg Chem*, 2018, **57**, 11252-11263.
41. P. J. Burns, J. M. Cox and J. R. Morrow, *Inorg Chem* , 2017, **56**, 4545-4554.
42. P. B. Tsitovich, F. Gendron, A. Y. Nazarenko, B. N. Livesay, A. P. Lopez, M. P. Shores, J. Autschbach and J. R. Morrow, *Inorg Chem*, 2018, **57**, 8364-8374.
43. P. B. Tsitovich, J. A. Spernyak and J. R. Morrow, *Angew Chem Int Edit*, 2013, **52**, 13997-14000.
44. P. B. Tsitovich, J. M. Cox, J. A. Spernyak and J. R. Morrow, *Inorg Chem*, 2016, **55**, 12001-12010.
45. M. M. Ali, M. Woods, E. H. Suh, Z. Kovacs, G. Tircso, P. Y. Zhao, V. D. Kodibagkar and A. D. Sherry, *J Biol Inorg Chem*, 2007, **12**, 855-865.
46. Y. K. Wu, S. R. Zhang, T. C. Soesbe, J. Yu, E. Vinogradov, R. E. Lenkinski and A. D. Sherry, *Magn Reson Med*, 2016, **75**, 2432-2441.
47. G. Ferrauto, F. Beauprez, E. Di Gregorio, C. Carrera, S. Aime, E. Terreno and D. Delli Castelli, *Dalton Trans*, 2019, **48**, 5343-5351.
48. O. M. Evbuomwan, G. Kiefer and A. D. Sherry, *Eur J Inorg Chem*, 2012, DOI: 10.1002/ejic.201101369, 2126-2134.
49. O. M. Evbuomwan, M. E. Merritt, G. E. Kiefer and A. D. Sherry, *Contrast Media Mol I*, 2012, **7**, 19-25.
50. F. Carniato, G. Ferrauto, M. Munoz-Ubeda and L. Tei, *Magnetochemistry*, 2020, **6**, 38; doi:10.3390/magnetochemistry6030038
51. M. M. Ali, B. Yoo and M. D. Pagel, *Mol Pharmaceut*, 2009, **6**, 1409-1416.